# Intensification of Hurricane Sally (2020) over the Mississippi River Plume

EFFY B. JOHN,[a] KARTHIK BALAGURU,[a] L. RUBY LEUNG,[a] GREGORY R. FOLTZ,[b] ROBERT D. HETLAND,[a] AND SAMSON M. HAGOS[a]

[a] *Pacific Northwest National Laboratory, Richland, Washington*
[b] *NOAA/Atlantic Oceanographic and Meteorological Laboratory, Miami, Florida*

(Manuscript received 4 November 2022, in final form 18 May 2023, accepted 24 May 2023)

ABSTRACT: Tropical Cyclone (TC) Sally formed on 11 September 2020, traveled through the Gulf of Mexico (GMX), and intensified rapidly before making landfall on the Alabama coast as a devastating category-2 TC with extensive coastal and inland flooding. In this study, using a combination of observations and idealized numerical model experiments, we demonstrate that the Mississippi River plume played a key role in the intensification of Sally near the northern Gulf Coast. As the storm intensified and its translation slowed before landfall, sea surface cooling was reduced along its track, coincident with a pronounced increase in SSS. Further analysis reveals that TC Sally encountered a warm Loop Current eddy in the northern GMX close to the Mississippi River plume. Besides deepening the thermocline, the eddy advected low-salinity Mississippi River plume water into the storm's path. This resulted in the development of strong upper-ocean salinity stratification, with a shallow layer of freshwater lying above a deep, warm "barrier layer." Consequently, TC-induced mixing and the associated sea surface cooling were reduced, aiding Sally's intensification. These results suggest that the Mississippi River plume and freshwater advection by the Loop Current eddies can play an important role in TC intensification near the U.S. Gulf Coast.

KEYWORDS: Atmosphere-ocean interaction; Hurricanes/typhoons; Intensification

## 1. Introduction

Tropical cyclones (TCs) cause significant damages to life and property worldwide, including in the United States (Pielke and Landsea 1999; Emanuel 2003; Pielke et al. 2008; Klotzbach et al. 2018). TCs intensify primarily by extracting heat energy from the ocean. Warm sea surface temperatures (SSTs) are conducive to TC intensification because they enhance enthalpy fluxes at the air–sea interface (Emanuel 1999; Cione and Uhlhorn 2003). However, the strong winds associated with TCs induce intense vertical mixing, and the cyclonic rotation of the storm can generate upwelling due to diverging Ekman transport. This results in a cooling of the sea surface that acts as a negative feedback on the storm's intensity (Price 1981; Emanuel 1999; Schade and Emanuel 1999; Zedler et al. 2002; D'Asaro 2003; Emanuel 2003; Lloyd et al. 2011). TC-induced SST cooling depends on several factors such as the size, intensity, and translation speed of the storm as well as the oceanic conditions (e.g., SST, depth of thermocline, salinity stratification). The heat content of the underlying ocean also affects TC-induced SST cooling and intensification. Oceanic conditions in the Gulf of Mexico (GMX) can be favorable for intensification of storms, particularly over the Loop Current and Loop Current eddies, due to warm SSTs and a deep thermocline, resulting in high upper-ocean heat content. Consequently, several storms, such as Opal (1995), Katrina (2005), and Harvey (2017) intensified into major TCs after traveling over warm core eddies. The influence of warm core eddies on TC intensification is well known (Shay et al. 2000; Scharroo et al. 2005; Potter et al. 2019).

Apart from temperature, salinity can also exert control on the upper-ocean density structure in the vicinity of large rivers. Enhanced salinity-induced density stratification causes TC-generated vertical mixing and entrainment of cooler water into the mixed layer to be reduced significantly, referred to as a barrier layer effect (Balaguru et al. 2012; Neetu et al. 2012). This reduction in SST cooling under the storm is favorable for TC intensification. Consequently, the role of river plumes in barrier layer formation and its impact on storms have been studied previously using observations and numerical model simulations (Balaguru et al. 2012; Grodsky et al. 2012; Domingues et al. 2015; Rudzin et al. 2019; Reul et al. 2021; Sun et al. 2021). For example, a study by Reul et al. (2014) showed that in the Amazon–Orinoco plume region, SST cooling associated with TCs is reduced by 50% compared to the surrounding waters. In the Bay of Bengal, the haline stratification induced by freshwater input from the summer monsoon rainfall and river runoff causes a 40% reduction in TC-induced SST cooling (Neetu et al. 2012). Hong et al. (2022) reported that the freshwater and the salinity-induced barrier layer associated with the Changjiang River plume could reduce the SST cooling for TCs that pass through the East China Sea.

The extremely active 2020 Atlantic TC season was destructive, with eight TCs making devastating landfalls in the GMX (Dzwonkowski et al. 2021). Among them, Sally was a slow-moving storm that rapidly intensified near the Mississippi River plume and made landfall on the Alabama coast with record flooding from heavy rainfall. Sally was a category-2 TC based on its lifetime maximum intensity of 49 m $s^{-1}$ (110 mph). It

Supplemental information related to this paper is available at the Journals Online website: https://doi.org/10.1175/WAF-D-22-0191.s1.

*Corresponding author*: Effy B. John, effy.john@pnnl.gov

DOI: 10.1175/WAF-D-22-0191.1

caused several fatalities and inflicted damages of about $7 billion (U.S. dollars) in the United States (Berg and Reinhart 2021). Recently, Emanuel (2017) showed using theory and models that under global warming, there is a higher chance for TCs to undergo rapid intensification just before landfall. The most striking feature of Sally's evolution was its rapid intensification phase that coincided with a slowdown in forward speed as it approached the coast. Typically, a TC with slow (≈2 m $s^{-1}$) translation speed induces more SST cooling, which can potentially weaken the storm (Geisler 1970). However, interestingly, Sally intensified near the Mississippi River plume despite moving slowly and intense winds were observed until landfall. Recent studies by (Dzwonkowski et al. 2021, 2022) examined the near-shelf oceanic conditions in the Mississippi Bight and concluded that a sequence of events occurred prior to TC Sally that led to storm-favorable upper-ocean thermal conditions over the continental shelf. Similarly, Gramer et al. (2022) analyzed three TCs in the GMX including Sally and concluded that coastal downwelling increased the enthalpy fluxes as they approached land and thus created conditions conducive for TC intensification. These studies mainly focused on the near-shelf temperature conditions and the associated processes within the shelf region. However, the potential role of salinity stratification in the intensification of TC Sally has not been explored. It is important to understand the role of salinity stratification on TC-induced mixing in the northern GMX because this is a region where there is considerable freshwater discharge from the Mississippi River. On average, the spatial extent of the Mississippi River plume increases during the summer season peaking in the month of July (da Silva and Castelao 2018). The following months of August–October represent the climatological peak of the Atlantic TC season. Therefore, variations in the upper ocean freshening due to the Mississippi River discharge may have some implications for the strength of TCs in the northern GMX. In this work we aim to identify whether salinity variations associated with the Mississippi River plume influenced Sally's SST response and facilitated its intensification. We address this using observations and numerical model simulations.

## 2. Methods

### a. Data

Best track data from International Best Track Archive for Climate Stewardship (IBTrACS; Knapp et al. 2018) are used to obtain TC information, such as storm position and intensity. We also use daily optimally interpolated SST from Group for High-Resolution Sea Surface Temperature (GHRSST) at a 0.05° spatial resolution. In this study, the merged satellite SSS data obtained from European Space Agency (ESA) Climate Change Initiative Sea Surface Salinity (CCI 3.21 SSS) project are used (Boutin et al. 2021, https://catalogue.ceda.ac.uk/uuid/fad2e982a59d44788eda09e3c67ed7d5). This merged dataset combines Soil Moisture and Ocean Salinity (SMOS) and Soil Moisture Active Passive (SMAP) satellite retrievals and provides Level 4 (L4) gridded estimates of sea surface salinity (SSS) which may improve the spatial resolution of large mesoscale SSS features. Vertical ocean temperature and salinity profiles obtained from Hybrid Coordinate Ocean Model (HYCOM) Global Ocean Forecast System version 3.1 analysis (www.hycom.org) are used extensively in this study. This dataset has a horizontal resolution of 1/12° (≈9 km) and vertical resolution ranging from 2 to 10 m in the upper 100 m with higher resolution near the surface. Furthermore, data from an Argo float (AOML Float Number 4903254) are used to analyze the temperature and salinity conditions near Sally's path. This float was located roughly 20 km to the west of the track of the storm's center. The European Centre for Medium-Range Weather Forecasts (ECMWF) reanalysis dataset (ERA5) is used to examine the prestorm atmospheric conditions (two days before the passage of the storm) along Sally's track (Hersbach et al. 2020). Vertical wind shear is evaluated as the vector magnitude of the difference between winds at the 850- and 200-hPa levels. Relative humidity and air temperature are obtained between 700 and 925 hPa for the computation of moist static energy. The midtroposphere relative humidity at 600 hPa is also examined. All variables are averaged over a 1° box centered on the TC location.

We explored the impact of salinity on vertical mixing and TC-induced SST cooling using the Price–Weller–Pinkel (PWP) one-dimensional ocean mixed layer model (Price et al. 1986). The model is initialized with temperature and salinity profiles obtained from the HYCOM analysis. We obtained temperature and salinity profiles from a location along the track of TC Sally where strong salinity stratification was observed (29°N, 88°W). These profiles are used to initialize the PWP model in the control experiment, while in the sensitivity experiment, we initialize the PWP model with the same temperature profile and surface forcing but with a vertically uniform salinity of 35.5 psu. Therefore, the difference in evolution of SST in the experiments initialized with and without salinity stratification shows the impact of salinity on the SST cooling induced by Sally. For all experiments, the surface solar radiation and net surface heat flux were set to zero to isolate the role of ocean stratification in the SST cooling. An idealized surface wind profile for TC Sally was generated and used, following the method of DeMaria (1987). Here, we assume that the surface wind field is axisymmetric, with the wind speed determined as a function of the storm's maximum wind speed, radius of maximum winds, and distance from the storm's center. For further details regarding the development of the wind profile, see Balaguru et al. (2015). The PWP model's vertical resolution was 1 m, and we used a time step of 15 min. The maximum wind speed was set to 85 kt (1 kt ≈ 0.51 m $s^{-1}$) and the translation speed to 3 m $s^{-1}$, and a transect of wind velocity 20 km to the west of the storm's track was used to force the PWP model, consistent with the location of the Argo profile used to initialize the model.

### b. Calculations

Following Balaguru et al. (2015), the dynamic temperature ($T_{dy}$), or the temperature averaged over the variable mixing length ($L$), is calculated as

$$T_{dy} = \frac{1}{L}\int_0^L T(z)\,dz, \tag{1}$$

where $T(z)$ is the temperature as a function of depth $z$.

The mixing length ($L$) is defined as

$$L = h + \left(\frac{2\rho_o u_*^3 t}{\kappa g \alpha}\right)^{1/3}, \quad (2)$$

where $h$ is the initial mixed layer depth (MLD), $\rho$ is the seawater density, $u_*$ is the friction velocity (which may be calculated as $\sqrt{\tau/\rho}$, with $\tau$ being the surface windstress), $t$ is the time of mixing under the storm, $\kappa$ is the von Kármán constant, $g$ is the acceleration due to gravity, and $\alpha$ is the rate of increase of density with depth beneath the mixed layer.

The TC-induced cold wake $\Delta T$ can be represented as

$$\Delta T = T_{\mathrm{dy}} - \mathrm{SST}. \quad (3)$$

Tropical cyclone heat potential (TCHP) is calculated as the temperature integrated from the surface to the depth of the 26°C isotherm:

$$\mathrm{TCHP} = \rho C_p \int_0^{Z_{26}} [T(z) - 26] dz, \quad (4)$$

where $\rho$ is the seawater density, $C_p$ is the seawater specific heat capacity, $T(z)$ is the temperature, and $Z_{26}$ is the depth of the 26°C isotherm (Shay et al. 2000). All of the above calculations are done using HYCOM analysis data.

To demonstrate the influence of salinity stratification in the intensification of Sally, we calculated the dynamic potential intensity (DPI) using $T_{\mathrm{dy}}$. Following (Balaguru et al. 2015) DPI is calculated as

$$V_{\mathrm{max}}^2 = \frac{T_{\mathrm{dy}} - T_0}{T_0} \frac{C_K}{C_D} (k_{\mathrm{SST}} - k), \quad (5)$$

where $V_{\mathrm{max}}$ is the maximum intensity of the TC, $T_0$ is the outflow temperature, $C_D$ is the coefficient of drag, $C_K$ is the coefficient of enthalpy exchange, $k_{\mathrm{SST}}$ is the enthalpy of air in contact with the sea surface, $k$ is the specific enthalpy of air near the surface in the storm environment, and the value of $C_K/C_D$ is set to 0.9. To understand the significance of salinity for storm intensification, DPI is calculated using the full $T_{\mathrm{dy}}$ and the temperature-only $T_{\mathrm{dy}}$ with the difference between them representing the salinity effect Foltz and Balaguru (2016). Note that replacing $T_{\mathrm{dy}}$ with SST in Eq. (5) leads to the original potential intensity (PI) formulation of Emanuel (1999).

The moist static energy (MSE), which comprises the enthalpy, potential energy, and latent energy, is defined as

$$\mathrm{MSE} = C_p T + gz + L_v q, \quad (6)$$

where $C_p$ is specific heat at constant pressure, $T$ is air temperature, $g$ is gravitational acceleration, $z$ is height, $L_v$ is latent heat of vaporization, and $q$ is water vapor mixing ratio.

## 3. Results

### a. Synoptic overview of TC Sally

Figure 1a shows the track and intensity of TC Sally. The storm originated as a tropical depression between Andros Island and Bimini in the Bahamas on 11 September 2020 and entered the southeastern GMX on 12 September 2020 as a tropical storm. Sally intensified rapidly from 50 to 75 kt (category-1 TC) over an 18-h period on 14 September 2020 while it was moving northwestward over the GMX (Fig. 1a). There was a considerable reduction in Sally's translation speed and thereafter Sally turned north toward the northern Gulf Coast (Berg and Reinhart 2021). Sally intensified again just before its landfall over the Alabama coast on 16 September with its intensity increasing from 70 to 95 kt (category 2). Sally caused heavy rainfall (≈75 cm) and significant flooding along with wind damage in coastal towns. In this study, we examine the upper ocean conditions which led to the initial intensification of TC Sally which occurred in the deep GMX on 14 September.

We begin our analysis by examining the synoptic conditions along the track of Sally. The environmental factors considered here include SST, wind shear, midtropospheric relative humidity and moist static energy. A near-uniform SST of about 29.25°–29.5°C is observed in the GMX along the storm's path (Fig. 1b). Though the prevailing SSTs were sufficient for TC intensification, a substantial increase in SST was not observed when Sally intensified rapidly. Another parameter that significantly modulates TC intensity is vertical wind shear. TCs typically intensify when the ambient vertical shear is low (Simpson and Riehl 1958; Erickson 1974; Merrill 1988). Wind shear gradually increased from about 5 to 17 m $s^{-1}$ along Sally's path (Fig. 1c). Hence, while shear was initially favorable for intensification (Kaplan et al. 2015), it became less conducive in the later part of Sally's track (Fig. 1c). Relative humidity in the midtroposphere is another critical factor that affects TC intensification. Higher values of relative humidity (moist atmosphere) indicate a more favorable environment for TC intensification (DeMaria and Kaplan 1994; Gray 1968). Figure 1c shows the relative humidity at 600 hPa along the track of TC Sally. The midtroposphere was nearly saturated, with relative humidity varying between 70% and 90% except for a slight decrease in certain locations (Fig. 1c). We also calculated MSE along the storm's track. Generally, large values of MSE support strengthening of storms. However, MSE does not change substantially along the track of Sally (Fig. 1c). These results show that neither SST nor the atmospheric state can explain the sudden increase in Sally's intensity. Hence, we next examine the potential role of ocean subsurface conditions in TC Sally's intensification.

### b. Upper-ocean response to TC Sally

In this section, we examine the upper-ocean temperature and salinity responses to Sally's passage. Figure 2 shows spatial maps of differences in SST and SSS between 16 September (the day of landfall) and 12 September (the day Sally formed). The magnitude of SST cooling increased as the storm moved northwestward. However, sea surface cooling was smaller during the phase when the TC's winds were stronger and its translation was slower (Figs. 2a,b). The observed along-track translation speed and intensity of Sally obtained from IBTrACS are shown in Fig. 3. Usually, slow moving storms are affected more strongly by sea

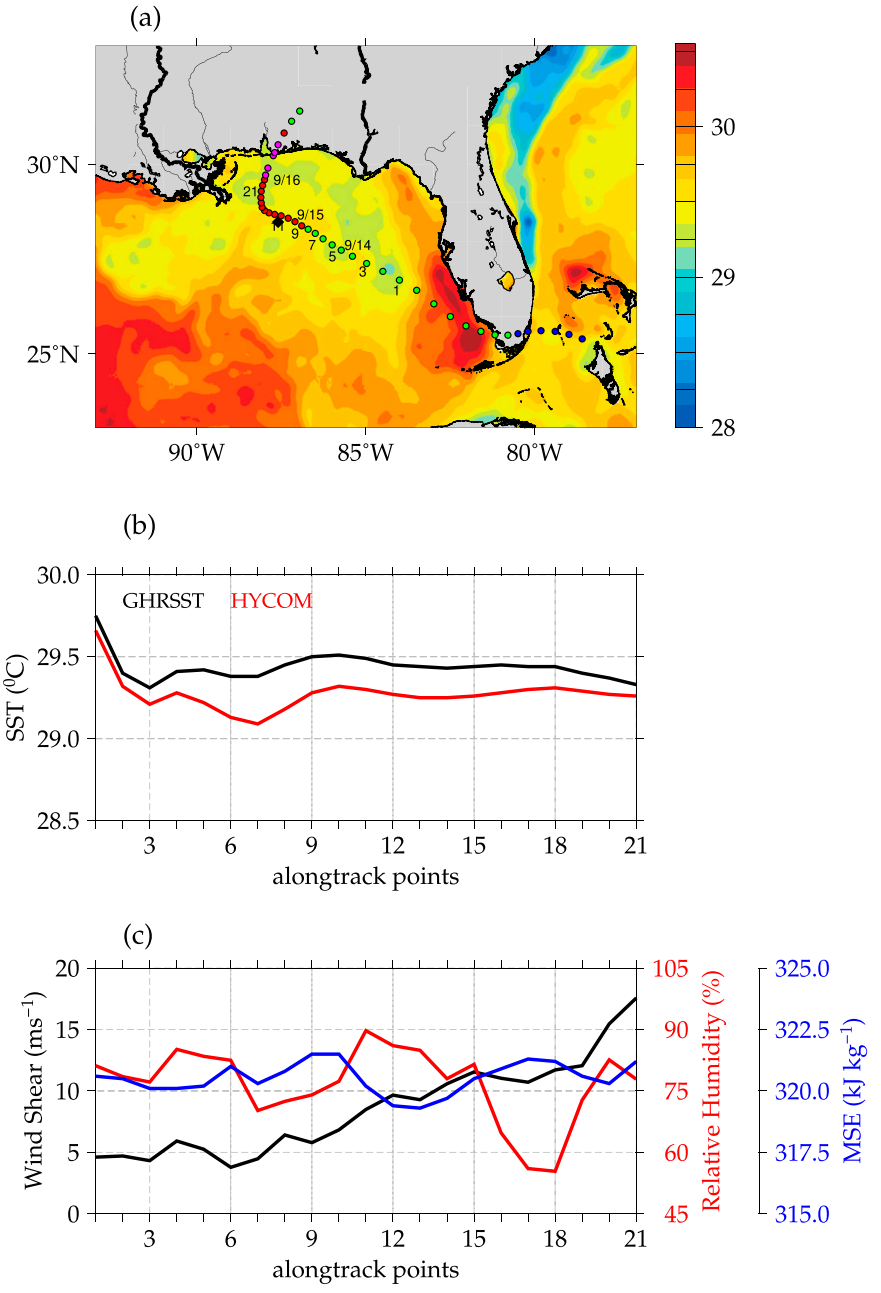


FIG. 1. (a) Spatial map of GHRSST SST (°C) on 12 Sep 2020 with the track of TC Sally overlaid. Each point represents the 3-h location of the storm with the intensity shown based on the Saffir–Simpson hurricane wind scale [tropical depression (blue circle), tropical storm (green circle), category 1 (red circle), and category 2 (magenta circle)]. The location of Argo is shown by black diamond symbol. Along-track (b) SST (°C) using GHRSST (black line) and HYCOM (red line), (c) wind shear (m $s^{-1}$), (d) relative humidity (%), and (e) moist static energy (kJ $kg^{-1}$) for TC Sally. Prestorm atmospheric conditions are calculated from 2 days before the passage of storm at each location.

surface cooling because of upwelling that occurs in addition to vertical mixing (Geisler 1970), and this acts as a negative feedback on the storm's intensity (Mei et al. 2012). Surface salinity increased by about 1 psu in the region of reduced SST cooling (Figs. 2c,d). The spatial pattern of SSS increase near the Mississippi River plume after the passage of Sally is consistent in both observations and HYCOM analysis (Figs. 2c,d).

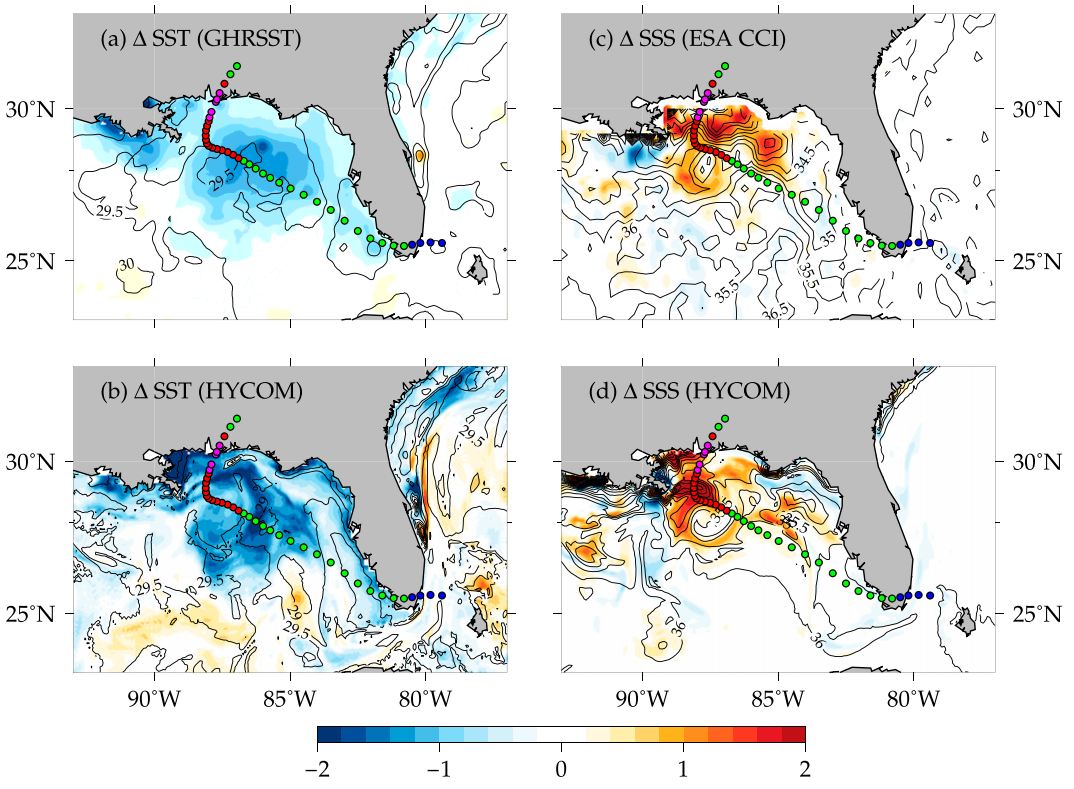


FIG. 2. Spatial map of SST (°C) difference between 16 and 12 Sep from (a) GHRSST and (b) HYCOM analysis. (c),(d) As in (a) and (b), but for SSS (psu) from CCI v3.2.1 and HYCOM analysis. Contour lines in (a) and (b) represent SST on 12 Sep from the GHRSST and HYCOM analysis, respectively. Contour lines in (c) and (d) represent SSS on 12 Sep from the CCI v3.2.1 and HYCOM analysis, respectively.

### c. *Subsurface oceanic conditions*

To better understand the upper-ocean temperature and salinity response to TC Sally, we analyze the prevailing subsurface oceanic conditions in the GMX along the storm's track. Figures 3b and 3c show the prestorm subsurface temperature and salinity conditions along the track during 12 September 2020. The vertical profiles of temperature depict warm water (>29°C) in the upper layers of the ocean. The warm water above 29°C extended to a depth of ≈30 m at the beginning of the track, then it shoaled to around 15 m. However, in the region where Sally intensified rapidly, the warmth extended again to a depth of ≈30 m. The depth of the 26°C isotherm was ≈60 m in this region. It is worth noting that the reduction in SST cooling begins in this region. Also, the thermocline started deepening from 40 to 60 m along the track of the TC. Several studies have shown that the depth of the 26°C isotherm, which broadly indicates the amount of heat stored in the upper ocean, is critical for fueling the TC heat engine (Shay et al. 2000). In regions with a deep thermocline, TC-induced mixing brings less cold water into the mixed layer, causing a reduction in the SST cooling and thus favoring TC intensification. Here, we attribute the initial decrease in SST cooling observed along the track of Sally to the deeper thermocline.

Apart from the ocean thermal structure, upper-ocean salinity stratification also influences storm-induced oceanic mixing and thus the SST response (Rudzin et al. 2018). Hence, it is important to understand the influence of the observed upper-ocean salinity stratification on Sally's reduced SST cooling. Figure 3c shows vertical profiles of salinity along the track of Sally. Freshwater (<34 psu) is observed extending up to a depth of 20 m along the latter part of the storm's track. Typically, in tropical freshwater regions the mixed layer shoals, leading to the formation of thick barrier layers above the thermocline (Lukas and Lindstrom 1991; Sprintall and Tomczak 1992). The strong salinity stratification within the pycnocline and the absence of a temperature gradient across the mixed layer base have a significant impact on air–sea interactions in the presence of barrier layers. Previous studies have reported that the barrier layer can weaken SST cooling, enhancing the enthalpy flux from the ocean to the atmosphere and thus favoring TC intensification (Balaguru et al. 2012; Rudzin et al. 2018; Balaguru et al. 2020).

### d. *Role of salinity stratification in the reduced SST cooling and TC intensification*

#### 1) CALCULATION OF $T_{DY}$

A detailed analysis of the role of salinity stratification in the reduction of TC-induced SST cooling was performed using the $T_{dy}$ framework (Balaguru et al. 2015). The $T_{dy}$ is defined as the column-integrated temperature from the surface to the depth of TC-induced mixing ($L$). The computation of mixing

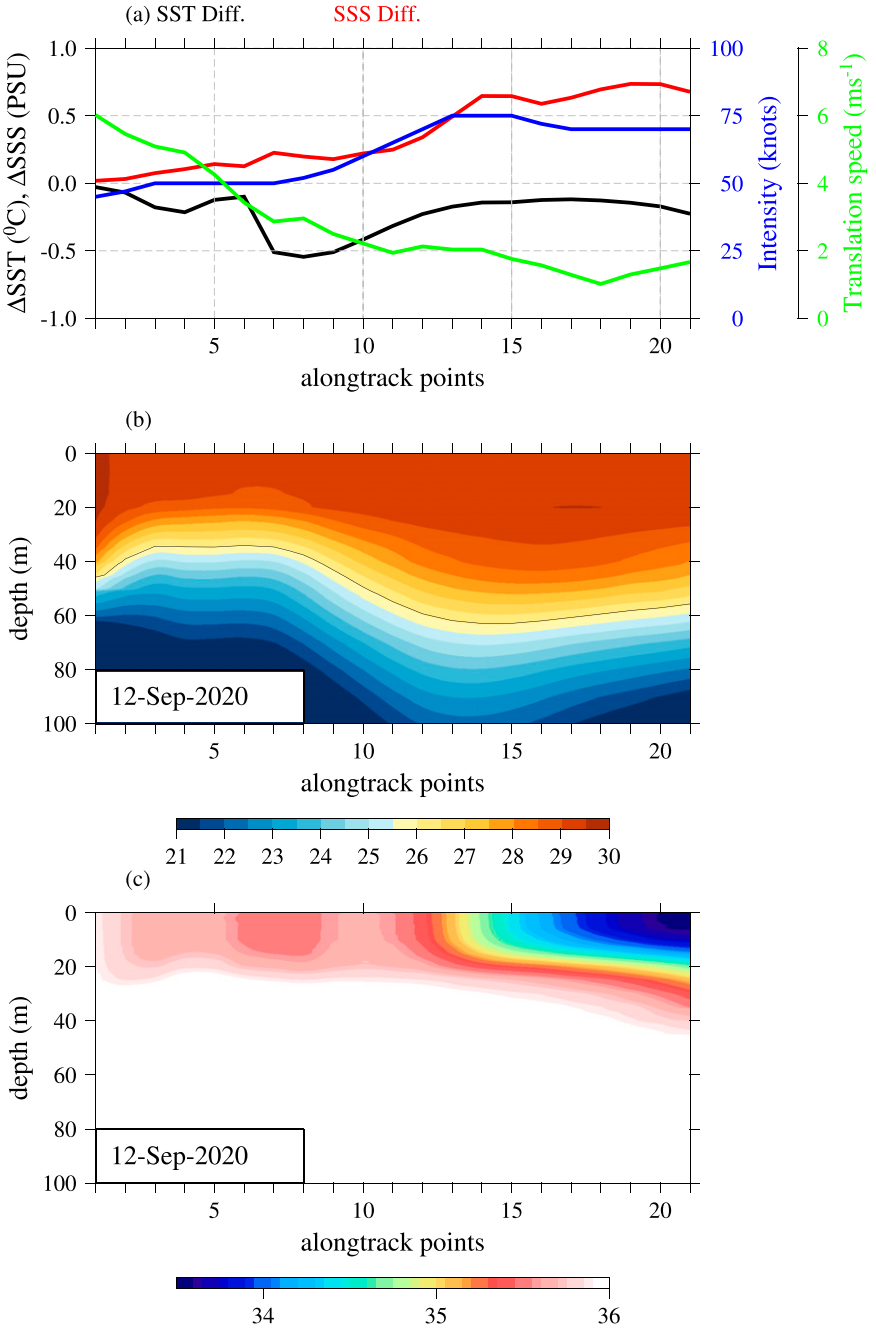


FIG. 3. (a) TC-induced changes in SST (°C; black line) and SSS (psu; red line) from HYCOM analysis, TC intensity (kt; blue line), and translation speed (m $s^{-1}$; green line) along the track of TC Sally. (b),(c) Vertical sections of prestorm temperature and salinity along the track of the storm, respectively. The black line in (b) represents the depth of the 26°C isotherm. Changes in SST (SSS) are estimated as the difference between SST (SSS) on the day of the TC and SST (SSS) on the previous day along the TC Sally's track.

length involves information about density stratification due to temperature and salinity, TC wind speed, and translation speed (Balaguru et al. 2015). Thus, $T_{dy}$, which accounts for both the storm state and upper-ocean conditions, is an estimate of the surface temperature felt by the TC, and the difference between $T_{dy}$ and SST is indicative of the TC-induced cold wake. To isolate the role of salinity, $T_{dy}$ is calculated with and without salinity stratification (Balaguru et al. 2016). More specifically, we compute the full $T_{dy}$ and the temperature-only $T_{dy}$, with the difference between them representing the impact of salinity

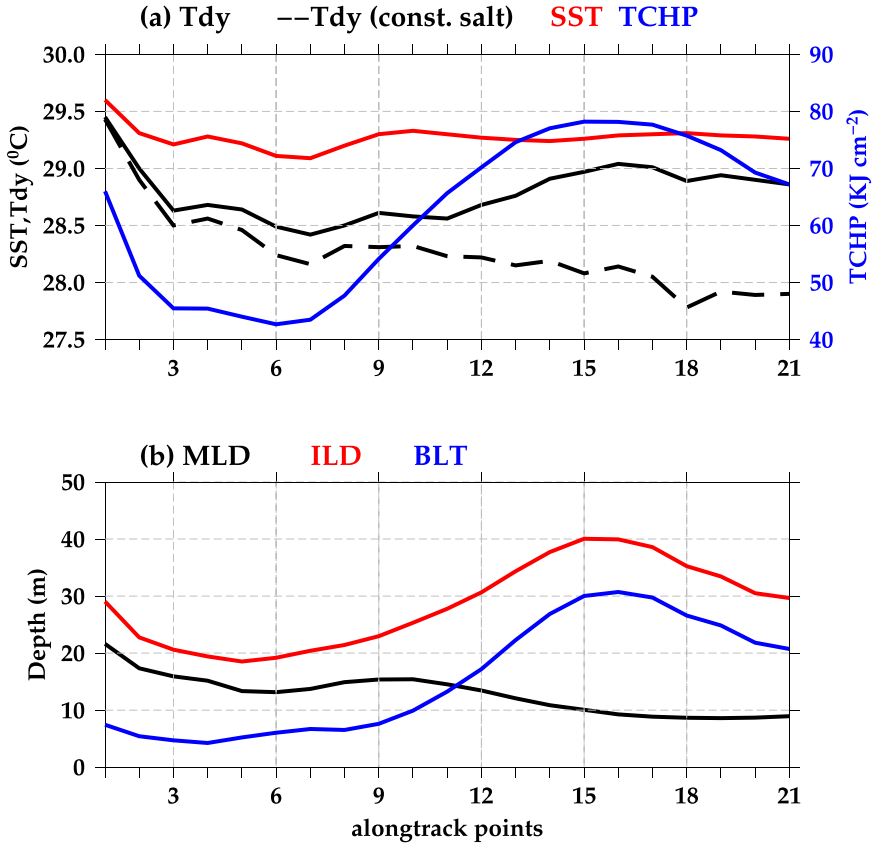


FIG. 4. (a) Along-track $T_{dy}$ (solid black line) with salinity stratification, $T_{dy}$ (dashed black line) without salinity stratification, SST (red line), and TCHP (blue line) of TC Sally calculated from HYCOM analysis. (b) Along-track mixed layer depth (m; black line), isothermal layer depth (m; red line), and barrier layer thickness (m; blue line) of TC Sally.

(Fig. 4a). From Fig. 4a, we observe that the TC-induced cooling (the difference between $T_{dy}$ and SST) was about 0.2°–0.75°C before encountering the fresh waters. Later, along the track of the storm, $T_{dy}$ increased from 28.4° to 29°C. Hence there is a reduction in SST cooling, with values ranging between 0.2° and 0.5°C along the track of the storm for locations with freshwater (locations 12–21). It is interesting to note that temperature-only $T_{dy}$ shows a steady decrease along the track. Therefore, without the effect of salinity stratification, the TC-induced SST cooling would have been considerably higher (≈1°–1.5°C). The magnitude of SST cooling reaches a minimum in the region where the barrier layer is thick (Fig. 4b), suggesting that even when the wind forcing increased and the translation speed decreased, the storm could not break through the stratification barrier. This resulted in reduced SST cooling. Note that none of the locations considered in this analysis corresponds to the continental shelf region.

Another interesting feature is the increase in TCHP associated with the deepening of the thermocline as observed in Fig. 3b. Generally, high (low) TCHP values with a deep (shallow) thermocline tend to produce less (more) SST cooling through a modulation of wind-induced vertical mixing. Along the track of TC Sally, TCHP increased from 40 to 80 kJ cm$^{-2}$ (Fig. 4a). In the western Atlantic basin, TCs tend to intensify where TCHP is larger than 50 kJ cm$^{-2}$ (Mainelli et al. 2008). In short, the deep thermocline and the presence of low saline water along Sally's track acted in concert to reduce SST cooling, and this likely resulted in the intensification of Sally. Note that there is a reduction in the magnitude of SST cooling of up to 1°C due to salinity stratification, emphasizing the importance of upper-ocean salinity.

To more clearly assess the role of prestorm salinity stratification in the SST response to TC Sally and to confirm the above explanation, we performed numerical experiments using the PWP model (Price et al. 1986). PWP is a one-dimensional ocean mixed layer model and has been used extensively to study TC-induced SST cooling and its response to TC intensification (Balaguru et al. 2015; Hlywiak and Nolan 2019). The evolution of the difference in SST in the PWP model experiments initialized with and without salinity stratification shows the impact of salinity on TC-induced SST cooling. The net TC-induced SST cooling is about −0.17°C in the control run, whereas it is nearly −1°C in the sensitivity experiment (Fig. 5). These results confirm that salinity stratification substantially reduced the SST cooling (0.83°C less cooling) induced by Sally and are in broad agreement with the results based on the $T_{dy}$ framework discussed

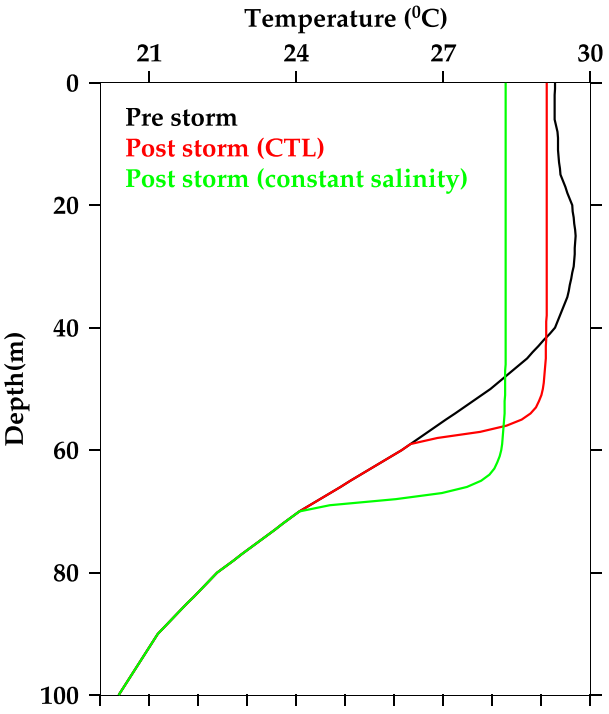


FIG. 5. Vertical profiles of temperature during prestorm (black line), poststorm obtained from control run (red line), and sensitivity experiment without salinity stratification (green line).

earlier. This is also consistent with the study by Reul et al. (2014), which found a reduction in SST cooling of about 35%–60% over the Amazon–Orinoco freshwater plume compared to outside the plume, with the magnitude depending on the intensity of TC winds.

#### 2) IN SITU OBSERVATIONS OF THE OCEANIC RESPONSE TO TC SALLY

In situ measurements of salinity and temperature from Argo floats offer key support for the role of salinity stratification in Sally's intensification. In this section we examine the subsurface hydrographic conditions from an Argo float that was located at 28.5°N, 87.6°W, approximately 20 km from Sally's path. Note that the Argo float had a sampling interval of 5 days. In this analysis, we obtained the temperature and salinity profiles on 5 September (9 days before the passage of the TC, day −9), 10 September (4 days before the passage of the TC, day −4) and 15 September (1 day after the passage of the TC, day 1). Figure 6 shows the subsurface temperature and salinity recorded by the float. The SSTs during day −9 and day −4 were 29.54° and 29.37°C, respectively. The prestorm vertical profiles of temperature did not change significantly (Figs. 6a,b). During day −4, ILD was 47 m, about 8 m deeper than on day −9 (39 m). Interestingly, after the passage of the storm, only a slight decrease in SST (0.26°C) was found, consistent with satellite observations. The vertical profiles of salinity exhibit considerable variability between day −9 and day −4, including a drop in SSS of 0.2 psu (Figs. 6a,b). Unlike day −9, a strong vertical salinity gradient is observed on day −4 with a rapid increase of salinity below the mixed layer. Due to the salinity effect, the MLD was shallower than 10 m, resulting in a thick barrier layer extending to a depth of more than 30 m. The Mississippi River plume presumably contributed to the observed barrier layer and strong salinity stratification. After the passage of the storm, an increase of 0.3 psu is observed. Also, after the passage of the storm, the mixed layer was thicker, resulting in a decrease of the barrier layer thickness (7.7 m, Fig. 6c). Another Argo float located at 27.95°N, 88.64°W, which is approximately 120 km to the west of the TC track, also showed very thick prestorm barrier layer (≈35 m, Fig. S1 in the online supplemental material) one day before the storm's arrival. After Sally's passage, the barrier layer was eroded mainly due to the deepening of the mixed layer. In the next section, we analyze the contribution of freshwater from the Mississippi River plume to the increase in salinity stratification.

To assess the impact of salinity stratification on the intensity of Sally, we calculated DPI with full $T_{dy}$ and the $T_{dy}$ without salinity stratification as shown in Fig. 7. The main advantage of using DPI is that it is based on mixing length $L$ which accounts for the storm state through $t$ and $u_*$ as well as ocean stratification through $\alpha$. In the initial phase of the storm (before 1800 UTC 14 September), with both PI and DPI being significantly higher than the intensity of the storm, the environment supported Sally's intensification. Later, when the storm's maximum intensity approximately equaled the PI, it could not intensify further highlighting the significance of PI. The agreement between PI and the DPI calculated using the full $T_{dy}$ in the later phase (after 1800 UTC 14 September) is interesting and likely points to the important role played by salinity in reducing storm-induced SST cooling. Further, there is a notable difference in the evolution of DPI calculated using full $T_{dy}$ and $T_{dy}$ without salinity stratification in the later phase of Sally. The DPI calculated without salinity stratification decreased (≈20 kt) compared to full DPI, which indicates that without salinity stratification the storm strength would likely have decreased as it approached the coast. These results underline the important role played by salinity in the reduced SST cooling and intensity of TC Sally.

### e. *Advection of freshwater from the Mississippi River plume*

The Mississippi River is the largest river in North America and is a major source of freshwater for the GMX (Hu et al. 2005). Several observational and numerical modeling studies described the spatial and temporal variability of the Mississippi River plume (Lohrenz et al. 1990; Green et al. 2006; Zhang et al. 2012, 2014; Luo et al. 2016). Unlike the Amazon–Orinoco River plume, which transports freshwater up to 1000 km away from the coast (Masson and Delecluse 2001; Coles et al. 2013), about half of the Mississippi River water emanating from the Mississippi Delta stays on the Texas–Louisiana continental shelf to the west, with the other half dispersing offshore or to the east (Dinnel and Wiseman 1986). Climatologically, the Mississippi River plume flows westward along the northwestern GMX shelf except during summer months when the plume tends to reverse and extend eastward due to a change in the wind direction from easterly to southerly (Morey et al. 2003a;

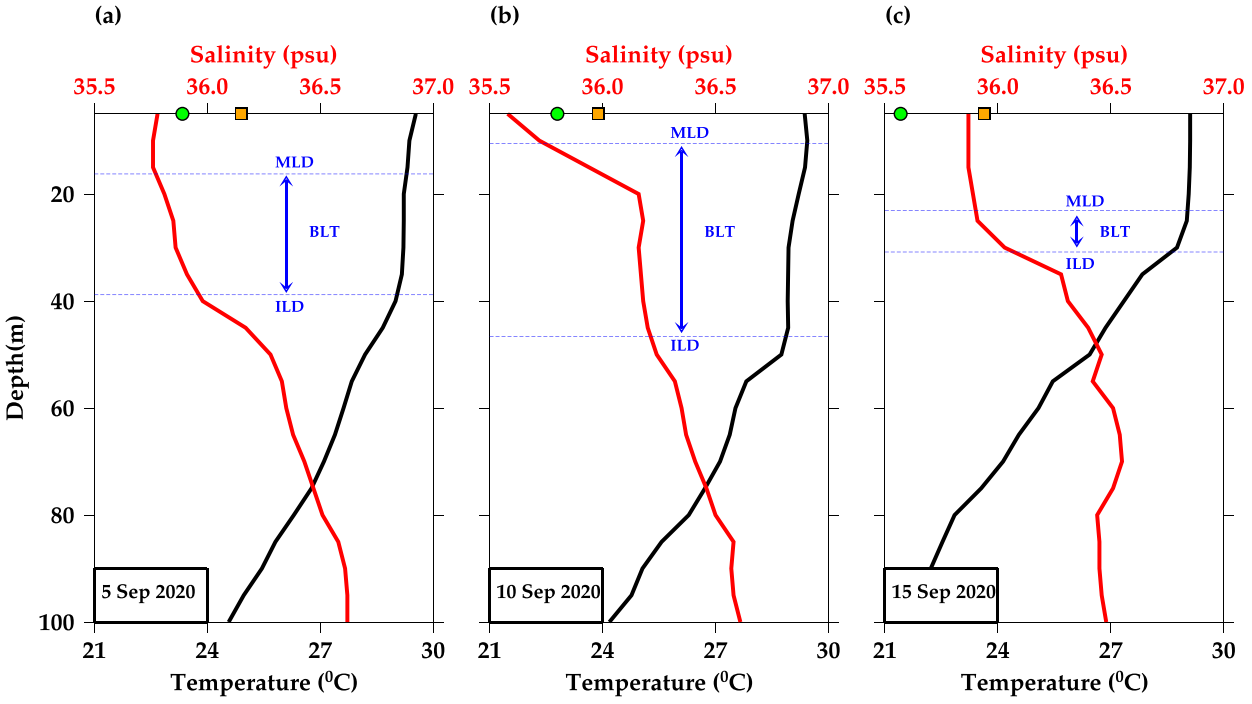


FIG. 6. Subsurface temperature (black) and salinity (red) profiles measured by Argo floats (4903254) on (a) 5, (b) 10, and (c) 15 Sep 2020, at 28.5°N, 87.6°W. The blue lines indicate the MLD and ILD, respectively, with the distance separating them being the BLT. SSS from CCI v3.21 and HYCOM is shown by a green circle and an orange square, respectively.

Zhang et al. 2014). Studies also showed that the plume may be driven offshore by winds or interaction with offshore eddies (Gilbert et al. 1996; Schiller and Kourafalou 2014). In the present study, to understand the role of freshwater advection from the Mississippi River plume in the northern GMX, snapshots of SSS from CCI v3.21 and surface currents from OSCAR data are examined from 3 to 16 September (Fig. 8).

The low-salinity water associated with the Mississippi River plume is clearly distinguishable from surrounding waters (Fig. 8). The Mobile River plume near the Alabama coast is unlikely to be a strong influence during this time; the maximum discharge in the month preceding TC Sally landfall was slightly less than 800 $m^3 s^{-1}$, whereas the discharge from the Mississippi was more than 10 times higher in the preceding month. The spatial map of SSS demonstrates strong interactions between the Mississippi River plume and offshore circulation processes. On 3 September, an anticyclonic eddy with a high-salinity core was seen in close proximity to the Mississippi River plume (Fig. 8a). Offshore transport of low-salinity water is observed along the northeastern edge of this eddy. On 5 September, the day before Sally formed,

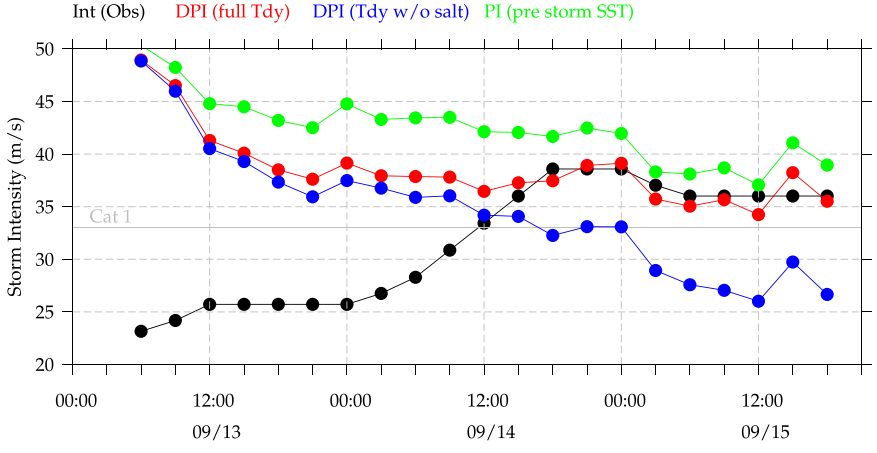


FIG. 7. Time series of observed storm intensity (black line) of Sally, DPI calculated using full $T_{dy}$ (red line), $T_{dy}$ without salinity stratification (blue line), and prestorm SST (green line).

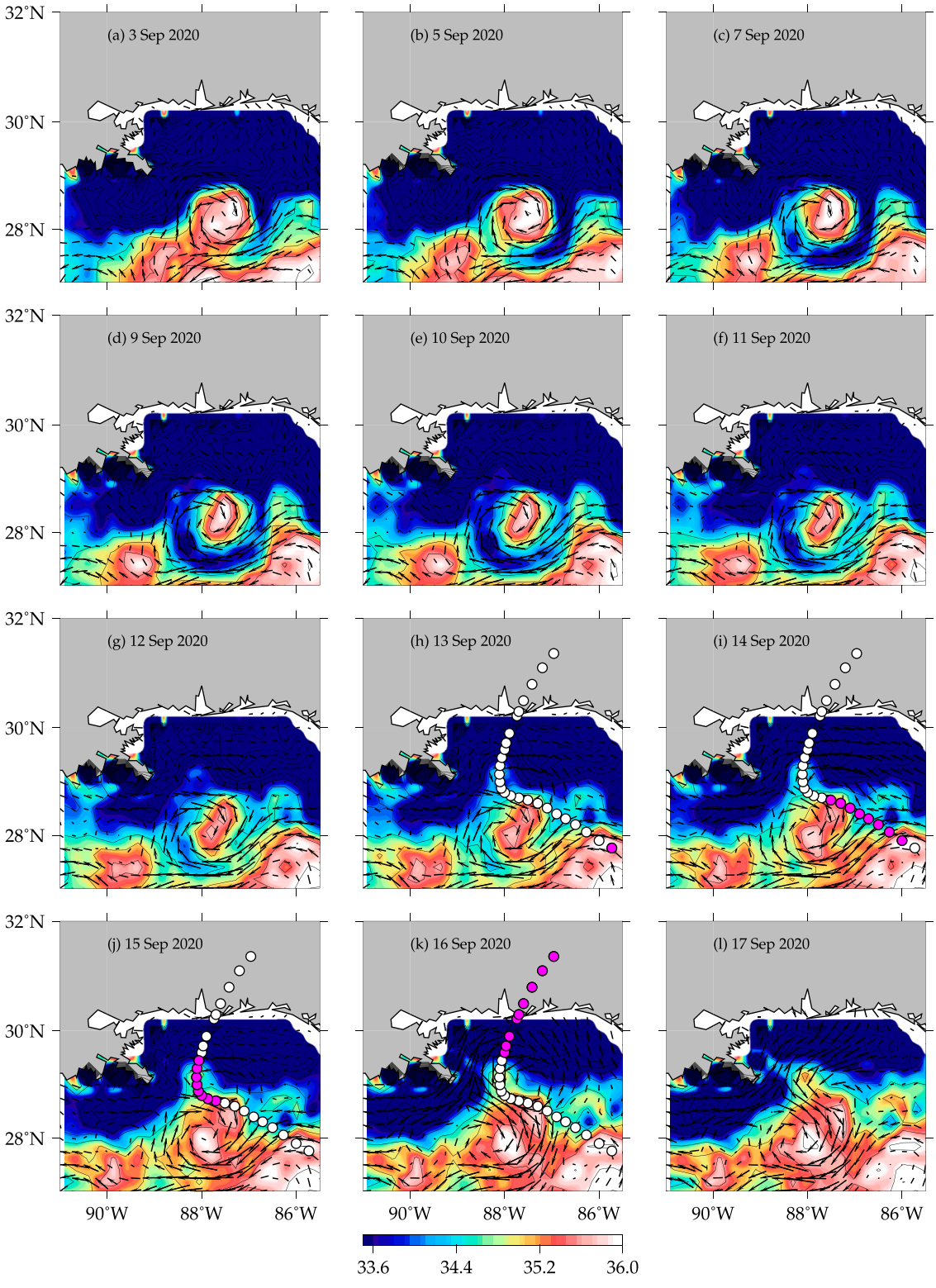


FIG. 8. Spatial map of daily CCI v3.21 SSS (psu; filled color) and OSCAR currents (m $s^{-1}$; vectors) in the northern GMX on (a) 3, (b) 5, (c) 7, (d) 9, (e)10, (f) 11, (g) 12, (h) 13, (i) 14, (j) 15, (k) 16, and (l) 17 Sep 2020. The track of TC Sally is also shown by white filled circles. The TC center location for each day is denoted by magenta circles.

the low-saline water was transported further south along the edge of this eddy (Fig. 8c). By 11 September the low saline water (<34 psu) from the plume can be observed surrounding the eddy's inner core nearly on all sides (Fig. 8f). This led to the formation of a ringlike feature of a low-salinity band around the eddy. On 14 September, Sally traversed over this filament of freshwater that was advected from the Mississippi River plume (Fig. 8i). The initial intensification of Sally occurred as it crossed this freshwater filament surrounding the eddy (≈1.5 psu fresher than surrounding open ocean waters) on 14 September. As the fresher water was rapidly transported within a few days, a strong vertical gradient of salinity formed, as is evident from the Argo float 6. A thermosalinograph (TSG) on board the ship *OREGON II*, which measured SSS across this region on 9 September 2020, also shows lower values of SSS, which provides additional evidence for the transport of freshwater from the Mississippi River plume before the arrival of Sally (Fig. S2). This low-salinity surface water along the edge of the anticyclonic eddy stratified the upper ocean and shoaled the mixed layer. The reduction in MLD, together with a deepened isothermal layer, led to the formation of a thick barrier layer. Subsequently, TC-induced vertical mixing and sea surface cooling were reduced, paving the way for Sally's intensification (25 kt in 24 h).

After the passage of the storm, the low-salinity band disappeared due to intense TC-induced mixing. Previous studies reported that Loop Current eddies play an important role in the transport of low-saline water from the Mississippi plume. Loop Current eddies have been found to transport Mississippi River plume water offshore, producing a freshwater lens and vertical salinity gradients in the upper ocean (da Silva and Castelao 2018). When Loop Current eddies reach close to the coast, freshwater can be entrained into the Gulf as thin filaments along their edges (Morey et al. 2003b; Walker et al. 2005). Export of freshwater filaments by eddies is a common occurrence in many regions (Cherian and Brink 2016). Thus, it is likely that the freshwater encountered by TC Sally along its path was entrained from the plume by a Loop Current eddy. To the best of our knowledge, the interaction between a TC and freshwater transported by an eddy, such as the one presented in this study, has not been documented in the GMX. This study points to the need for high spatiotemporal resolution datasets that can accurately resolve fine-scale salinity processes in the upper ocean and over the continental shelf.

## 4. Conclusions

Sally was a storm that entered the GMX and intensified rapidly just before making landfall. We analyzed the prestorm ocean conditions and distinct upper-ocean responses to TC Sally using observations and HYCOM analysis. Though many major TCs have made landfall in the northern GMX, few studies analyzed the contribution of low-salinity water from the Mississippi River plume in the weakening of TC-induced SST cooling and thus the intensification of storms. TC Sally induced less SST cooling (≈0.2°C) during the phase when it intensified (>63 kt) and moved slowly (<2 m $s^{-1}$) compared to when it was weaker and moved more rapidly. This is in contrast to studies showing that the magnitude of SST cooling increases with increasing intensity (Lloyd and Vecchi 2011; Vincent et al. 2014) and decreasing translation speed (Mei et al. 2012).

A near-uniform SST of about 29.5°C was observed along the track of the storm which is quite warm and well above the 27°C threshold for supporting TC intensification. Though warm SSTs are favorable for TC intensification, an increase in SST was not observed along the track of the storm. Furthermore, an increase in wind shear was observed, which was unfavorable for the intensification of the storm. Relative humidity and moist static energy did not change significantly along Sally's track. Despite the less conducive atmospheric environment, we found that the underlying subsurface oceanic conditions caused a weakening of the TC-induced cold wake, thereby promoting the intensification of the storm. The region where Sally intensified had warm (>29°C) and fresh (<35 psu) water with thick barrier layers attributable to freshwater input from the Mississippi River plume. We found that fresh waters from the river plume were advected by a Loop Current eddy as a thin filament along its northeastern edge. The TC happened to traverse the low-salinity water, resulting in a reduction in the magnitude of the TC-induced cold wake and thus favoring its intensification.

Even though several previous studies have been conducted to understand the barrier layer effect on TC-induced SST cooling and TC intensification in different regions across the world, little attention has been paid to the impact of the Mississippi River plume on TCs in the northern GMX. To our knowledge, no study has focused on the impact of salinity stratification associated with the Mississippi River plume on TC-induced SST cooling. The northern GMX is a region of paramount importance because many TCs transverse this area and make landfall over the Gulf Coast, resulting in significant damages to property and loss of life. Although our study focused on TC Sally, exploratory analysis reveals that other storms may also have been impacted by the Mississippi plume. For instance, we found that TC Issac (2012), a slow-moving TC that rapidly intensified to category-1 strength before landfall, was also influenced by the Mississippi River plume. As was observed during TC Sally, SST cooling decreased as Isaac strengthened (Fig. S3). Further analysis reveals that TC Issac also encountered fresh Mississippi River water transported by a Loop Current eddy, similar to what occurred for Sally (Fig. S3). A study by Jaimes et al. (2016) showed that TC Issac intensified in a region where the storm's center was flanked by two Loop Current eddies and they attributed the reduction in TC-induced SST cooling to the warmer waters that were advected over the northern branch of the Loop Current eddy. In our analysis, we found that in addition to the thermal conditions, salinity stratification aided the reduction in Isaac's SST cooling. Generally, fast-moving TCs are not exposed to the ocean at any given location for a long period of time and thus are expected to be less affected by the underlying oceanic conditions. However, in the case of slow-moving TCs, upper-ocean conditions affect TC-induced SST cooling and intensification. Our study points out that the high frequency events such as the advection of freshwater can influence the preconditioning of the ocean greatly which could affect TC intensification. Thus, the findings from this study may help explain why some relatively weaker storms with slow

translation intensify rapidly near the Mississippi River plume before making landfall.

The results from our study also call for salinity observations at high temporal and spatial scales in order to capture the complex processes associated with the dispersal of the Mississippi River plume in the northern GMX. Our study suggests that such observations may be used to constrain operational forecast models with the potential to improve intensity forecasts for landfalling TCs in the northern GMX. The current operational forecast models incorporate oceanic parameters such as SST and TCHP, which represent the amount of heat content in the underlying ocean to predict the intensification of TCs. Even though, in these models, the influence of thermal stratification of the ocean is considered, salinity effects are being ignored. Therefore, it is also important for the ocean models to incorporate the variations of Mississippi River discharge accurately in order to correctly represent the spatial and temporal variations of salinity associated with the river plume in the GMX. A better understanding of the oceanic processes in the northern GMX can help improve TC prediction and may offer more advanced warnings for people living near the coast.

*Acknowledgments.* This study was supported by the Office of Science, U.S. Department of Energy Biological and Environmental Research as part of the Regional and Global Model Analysis program area through the collaborative, multiprogram Integrated Coastal Modeling (ICoM) project and the Water Cycle and Climate Extremes Modeling (WACCEM) scientific focus area. The Pacific Northwest National Laboratory (PNNL) is operated for DOE by Battelle Memorial Institute under Contract DE-AC05-76RL01830. GF was supported by base funds to NOAA/AOML's Physical Oceanography Division. There is no conflict of interest.

*Data availability statement.* The sources for various observational data used in this study are as follows: TC data from International Best Track Archive for Climate Stewardship (IBTrACS, https://www.ncdc.noaa.gov/ibtracs/), ERA5 reanalysis data (https://www.ecmwf.int/en/forecasts/datasets/reanalysis-datasets/era5), GHRSST data (https://www.ghrsst.org/), and CCI v3.21 SSS data (https://data.ceda.ac.uk/neodc/esacci/sea_surface_salinity/data/v03.21/7days/2020).

## REFERENCES

Balaguru, K., P. Chang, R. Saravanan, L. R. Leung, Z. Xu, M. Li, and J.-S. Hsieh, 2012: Ocean barrier layers' effect on tropical cyclone intensification. *Proc. Natl. Acad. Sci. USA*, **109**, 14 343–14 347, https://doi.org/10.1073/pnas.1201364109.

——, G. R. Foltz, L. R. Leung, E. D. Asaro, K. A. Emanuel, H. Liu, and S. E. Zedler, 2015: Dynamic potential intensity: An improved representation of the ocean's impact on tropical cyclones. *Geophys. Res. Lett.*, **42**, 6739–6746, https://doi.org/10.1002/2015GL064822.

——, ——, ——, and K. A. Emanuel, 2016: Global warming-induced upper-ocean freshening and the intensification of super typhoons. *Nat. Commun.*, **7**, 13670, https://doi.org/10.1038/ncomms13670.

——, ——, ——, J. Kaplan, W. Xu, N. Reul, and B. Chapron, 2020: Pronounced impact of salinity on rapidly intensifying tropical cyclones. *Bull. Amer. Meteor. Soc.*, **101**, E1497–E1511, https://doi.org/10.1175/BAMS-D-19-0303.1.

Berg, R., and B. J. Reinhart, 2021: National Hurricane Center tropical cyclone report: Hurricane Sally (11–17 September 2020). NOAA Tech. Rep. AL192020, 69 pp., https://www.nhc.noaa.gov/data/tcr/AL192020_Sally.pdf.

Boutin, J., and Coauthors, 2021: Satellite-based sea surface salinity designed for ocean and climate studies. *J. Geophys. Res. Oceans*, **126**, e2021JC017676, https://doi.org/10.1029/2021JC017676.

Cherian, D. A., and K. H. Brink, 2016: Offshore transport of shelf water by deep-ocean eddies. *J. Phys. Oceanogr.*, **46**, 3599–3621, https://doi.org/10.1175/JPO-D-16-0085.1.

Cione, J. J., and E. W. Uhlhorn, 2003: Sea surface temperature variability in hurricanes: Implications with respect to intensity change. *Mon. Wea. Rev.*, **131**, 1783–1796, https://doi.org/10.1175//2562.1.

Coles, V. J., M. T. Brooks, J. Hopkins, M. R. Stukel, P. L. Yager, and R. R. Hood, 2013: The pathways and properties of the Amazon River plume in the tropical North Atlantic Ocean. *J. Geophys. Res. Oceans*, **118**, 6894–6913, https://doi.org/10.1002/2013JC008981.

D'Asaro, E. A., 2003: The ocean boundary layer below Hurricane Dennis. *J. Phys. Oceanogr.*, **33**, 561–579, https://doi.org/10.1175/1520-0485(2003)033<0561:TOBLBH>2.0.CO;2.

da Silva, C. E., and R. M. Castelao, 2018: Mississippi River plume variability in the Gulf of Mexico from SMAP and MODIS-Aqua observations. *J. Geophys. Res. Oceans*, **123**, 6620–6638, https://doi.org/10.1029/2018JC014159.

DeMaria, M., 1987: Tropical cyclone track prediction with a barotropic spectral model. *Mon. Wea. Rev.*, **115**, 2346–2357, https://doi.org/10.1175/1520-0493(1987)115<2346:TCTPWA>2.0.CO;2.

——, and J. Kaplan, 1994: Sea surface temperature and the maximum intensity of Atlantic tropical cyclones. *J. Climate*, **7**, 1324–1334, https://doi.org/10.1175/1520-0442(1994)007<1324:SSTATM>2.0.CO;2.

Dinnel, S. P., and W. J. Wiseman Jr., 1986: Fresh water on the Louisiana and Texas shelf. *Cont. Shelf Res.*, **6**, 765–784, https://doi.org/10.1016/0278-4343(86)90036-1.

Domingues, R., and Coauthors, 2015: Upper ocean response to Hurricane Gonzalo (2014): Salinity effects revealed by targeted and sustained underwater glider observations. *Geophys. Res. Lett.*, **42**, 7131–7138, https://doi.org/10.1002/2015GL065378.

Dzwonkowski, B., S. Fournier, G. Lockridge, J. Coogan, Z. Liu, and K. Park, 2021: Cascading weather events amplify the coastal thermal conditions prior to the shelf transit of Hurricane Sally (2020). *J. Geophys. Res. Oceans*, **126**, e2021JC017957, https://doi.org/10.1029/2021JC017957.

——, ——, ——, ——, ——, and ——, 2022: Hurricane Sally (2020) shifts the ocean thermal structure across the inner core during rapid intensification over the shelf. *J. Phys. Oceanogr.*, **52**, 2841–2852, https://doi.org/10.1175/JPO-D-22-0025.1.

Emanuel, K., 1999: Thermodynamic control of hurricane intensity. *Nature*, **401**, 665–669, https://doi.org/10.1038/44326.

——, 2003: Tropical cyclones. *Annu. Rev. Earth Planet. Sci.*, **31**, 75–104, https://doi.org/10.1146/annurev.earth.31.100901.141259.

——, 2017: Will global warming make hurricane forecasting more difficult? *Bull. Amer. Meteor. Soc.*, **98**, 495–501, https://doi.org/10.1175/BAMS-D-16-0134.1.

Erickson, C. O., 1974: Use of geostationary-satellite cloud vectors to estimate tropical cyclone intensity. Vol. 59, U.S. Department of Commerce, National Oceanic and Atmospheric Administration, 37 pp.

Foltz, G. R., and K. Balaguru, 2016: Prolonged El Niño conditions in 2014–2015 and the rapid intensification of hurricane Patricia in the eastern Pacific. *Geophys. Res. Lett.*, **43**, 10 347–10 355, https://doi.org/10.1002/2016GL070274.

Geisler, J. E., 1970: Linear theory of the response of a two layer ocean to a moving hurricane. *Geophys. Fluid Dyn.*, **1**, 249–272, https://doi.org/10.1080/03091927009365774.

Gilbert, P. S., T. N. Lee, and G. P. Podesta, 1996: Transport of anomalous low-salinity waters from the Mississippi River flood of 1993 to the Straits of Florida. *Cont. Shelf Res.*, **16**, 1065–1085, https://doi.org/10.1016/0278-4343(95)00056-9.

Gramer, L. J., J. A. Zhang, G. Alaka, A. Hazelton, and S. Gopalakrishnan, 2022: Coastal downwelling intensifies landfalling hurricanes. *Geophys. Res. Lett.*, **49**, e2021GL096630, https://doi.org/10.1029/2021GL096630.

Gray, W. M., 1968: Global view of the origin of tropical disturbances and storms. *Mon. Wea. Rev.*, **96**, 669–700, https://doi.org/10.1175/1520-0493(1968)096<0669:GVOTOO>2.0.CO;2.

Green, R. E., T. S. Bianchi, M. J. Dagg, N. D. Walker, and G. A. Breed, 2006: An organic carbon budget for the Mississippi River turbidity plume and plume contributions to air-sea $CO_2$ fluxes and bottom water hypoxia. *Estuaries Coasts*, **29**, 579–597, https://doi.org/10.1007/BF02784284.

Grodsky, S. A., and Coauthors, 2012: Haline hurricane wake in the Amazon/Orinoco plume: AQUARIUS/SACD and SMOS observations. *Geophys. Res. Lett.*, **39**, 2012GL053335, https://doi.org/10.1029/2012GL053335.

Hersbach, H., and Coauthors, 2020: The ERA5 global reanalysis. *Quart. J. Roy. Meteor. Soc.*, **146**, 1999–2049, https://doi.org/10.1002/qj.3803.

Hlywiak, J., and D. S. Nolan, 2019: The influence of oceanic barrier layers on tropical cyclone intensity as determined through idealized, coupled numerical simulations. *J. Phys. Oceanogr.*, **49**, 1723–1745, https://doi.org/10.1175/JPO-D-18-0267.1.

Hong, J.-S., J.-H. Moon, T. Kim, S. H. You, K.-Y. Byun, and H. Eom, 2022: Role of salinity-induced barrier layer in air-sea interaction during the intensification of a typhoon. *Front. Mar. Sci.*, **9**, 844003, https://doi.org/10.3389/fmars.2022.844003.

Hu, C., J. R. Nelson, E. Johns, Z. Chen, R. H. Weisberg, and F. E. Müller-Karger, 2005: Mississippi River water in the Florida Straits and in the Gulf Stream off Georgia in summer 2004. *Geophys. Res. Lett.*, **32**, L14606, https://doi.org/10.1029/2005GL022942.

Jaimes, B., L. K. Shay, and J. K. Brewster, 2016: Observed air-sea interactions in tropical cyclone Isaac over loop current mesoscale eddy features. *Dyn. Atmos. Oceans*, **76**, 306–324, https://doi.org/10.1016/j.dynatmoce.2016.03.001.

Kaplan, J., and Coauthors, 2015: Evaluating environmental impacts on tropical cyclone rapid intensification predictability utilizing statistical models. *Wea. Forecasting*, **30**, 1374–1396, https://doi.org/10.1175/WAF-D-15-0032.1.

Klotzbach, P. J., S. G. Bowen, R. Pielke Jr., and M. Bell, 2018: Continental U.S. hurricane landfall frequency and associated damage: Observations and future risks. *Bull. Amer. Meteor. Soc.*, **99**, 1359–1376, https://doi.org/10.1175/BAMS-D-17-0184.1.

Knapp, K. R., H. J. Diamond, J. P. Kossin, M. C. Kruk, and C. J. Schreck, III, 2018: International Best Track Archive for Climate Stewardship (IBTrACS) project, version 4. NOAA/National Centers for Environmental Information, https://www.ncei.noaa.gov/access/metadata/landing-page/bin/iso?id=gov.noaa.ncdc:C01552.

Lloyd, I. D., and G. A. Vecchi, 2011: Observational evidence for oceanic controls on hurricane intensity. *J. Climate*, **24**, 1138–1153, https://doi.org/10.1175/2010JCLI3763.1.

——, T. Marchok, and G. A. Vecchi, 2011: Diagnostics comparing sea surface temperature feedbacks from operational hurricane forecasts to observations. *J. Adv. Model. Earth Syst.*, **3**, M11002, https://doi.org/10.1029/2011MS000075.

Lohrenz, S. E., M. J. Dagg, and T. E. Whitledge, 1990: Enhanced primary production at the plume/oceanic interface of the Mississippi River. *Cont. Shelf Res.*, **10**, 639–664, https://doi.org/10.1016/0278-4343(90)90043-L.

Lukas, R., and E. Lindstrom, 1991: The mixed layer of the western equatorial Pacific Ocean. *J. Geophys. Res.*, **96**, 3343–3357, https://doi.org/10.1029/90JC01951.

Luo, H., A. Bracco, Y. Cardona, and J. C. McWilliams, 2016: Submesoscale circulation in the northern Gulf of Mexico: Surface processes and the impact of the freshwater river input. *Ocean Modell.*, **101**, 68–82, https://doi.org/10.1016/j.ocemod.2016.03.003.

Mainelli, M., M. DeMaria, L. K. Shay, and G. Goni, 2008: Application of oceanic heat content estimation to operational forecasting of recent Atlantic category-5 hurricanes. *Wea. Forecasting*, **23**, 3–16, https://doi.org/10.1175/2007WAF2006111.1.

Masson, S., and P. Delecluse, 2001: Influence of the Amazon River runoff on the tropical Atlantic. *Phys. Chem. Earth*, **26**, 137–142, https://doi.org/10.1016/S1464-1909(00)00230-6.

Mei, W., C. Pasquero, and F. Primeau, 2012: The effect of translation speed upon the intensity of tropical cyclones over the tropical ocean. *Geophys. Res. Lett.*, **39**, L07801, https://doi.org/10.1029/2011GL050765.

Merrill, R. T., 1988: Environmental influences on hurricane intensification. *J. Atmos. Sci.*, **45**, 1678–1687, https://doi.org/10.1175/1520-0469(1988)045<1678:EIOHI>2.0.CO;2.

Morey, S. L., P. J. Martin, J. J. O'Brien, A. A. Wallcraft, and J. Zavala-Hidalgo, 2003a: Export pathways for river discharged fresh water in the northern Gulf of Mexico. *J. Geophys. Res.*, **108**, 3303, https://doi.org/10.1029/2002JC001674.

——, W. W. Schroeder, J. J. O'Brien, and J. Zavala-Hidalgo, 2003b: The annual cycle of riverine influence in the eastern Gulf of Mexico basin. *Geophys. Res. Lett.*, **30**, 1867, https://doi.org/10.1029/2003GL017348.

Neetu, S., M. Lengaigne, E. M. Vincent, J. Vialard, G. Madec, G. Samson, M. R. Ramesh Kumar, and F. Durand, 2012: Influence of upper-ocean stratification on tropical cyclone-induced surface cooling in the Bay of Bengal. *J. Geophys. Res.*, **117**, C12020, https://doi.org/10.1029/2012JC008433.

Pielke, R. A., Jr., and C. N. Landsea, 1999: La Niña, El Niño, and Atlantic hurricane damages in the United States. *Bull. Amer. Meteor. Soc.*, **80**, 2027–2034, https://doi.org/10.1175/1520-0477(1999)080<2027:LNAENO>2.0.CO;2.

——., J. Gratz, C. W. Landsea, D. Collins, M. A. Saunders, and R. Musulin, 2008: Normalized hurricane damage in the United States: 1900–2005. *Nat. Hazards Rev.*, **9**, 29–42, https://doi.org/10.1061/(ASCE)1527-6988(2008)9:1(29).

Potter, H., S. F. DiMarco, and A. H. Knap, 2019: Tropical cyclone heat potential and the rapid intensification of Hurricane Harvey in the Texas bight. *J. Geophys. Res. Oceans*, **124**, 2440–2451, https://doi.org/10.1029/2018JC014776.

Price, J. F., 1981: Upper ocean response to a hurricane. *J. Phys. Oceanogr.*, **11**, 153–175, https://doi.org/10.1175/1520-0485(1981)011<0153:UORTAH>2.0.CO;2.

——, R. A. Weller, and R. Pinkel, 1986: Diurnal cycling: Observations and models of the upper ocean response to diurnal heating, cooling, and wind mixing. *J. Geophys. Res.*, **91**, 8411–8427, https://doi.org/10.1029/JC091iC07p08411.

Reul, N., Y. Quilfen, B. Chapron, S. Fournier, V. Kudryavtsev, and R. Sabia, 2014: Multisensor observations of the Amazon-Orinoco River plume interactions with hurricanes. *J. Geophys. Res. Oceans*, **119**, 8271–8295, https://doi.org/10.1002/2014JC010107.

——, B. Chapron, S. A. Grodsky, S. Guimbard, V. Kudryavtsev, G. R. Foltz, and K. Balaguru, 2021: Satellite observations of the sea surface salinity response to tropical cyclones. *Geophys. Res. Lett.*, **48**, e2020GL091478, https://doi.org/10.1029/2020GL091478.

Rudzin, J. E., L. K. Shay, and W. E. Johns, 2018: The influence of the barrier layer on SST response during tropical cyclone wind forcing using idealized experiments. *J. Phys. Oceanogr.*, **48**, 1471–1478, https://doi.org/10.1175/JPO-D-17-0279.1.

——, ——, and B. Jaimes de la Cruz, 2019: The impact of the Amazon–Orinoco river plume on enthalpy flux and air–sea interaction within Caribbean Sea tropical cyclones. *Mon. Wea. Rev.*, **147**, 931–950, https://doi.org/10.1175/MWR-D-18-0295.1.

Schade, L. R., and K. A. Emanuel, 1999: The ocean's effect on the intensity of tropical cyclones: Results from a simple coupled atmosphere–ocean model. *J. Atmos. Sci.*, **56**, 642–651, https://doi.org/10.1175/1520-0469(1999)056<0642:TOSEOT>2.0.CO;2.

Scharroo, R., W. H. F. Smith, and J. L. Lillibridge, 2005: Satellite altimetry and the intensification of Hurricane Katrina. *Eos, Trans. Amer. Geophys. Union*, **86**, 366–366, https://doi.org/10.1029/2005EO400004.

Schiller, R. V., and V. H. Kourafalou, 2014: Loop current impact on the transport of Mississippi River waters. *J. Coastal Res.*, **30**, 1287–1306, https://doi.org/10.2112/JCOASTRES-D-13-00025.1.

Shay, L. K., G. J. Goni, and P. G. Black, 2000: Effects of a warm oceanic feature on Hurricane Opal. *Mon. Wea. Rev.*, **128**, 1366–1383, https://doi.org/10.1175/1520-0493(2000)128<1366:EOAWOF>2.0.CO;2.

Simpson, R., and R. Riehl, 1958: Mid-tropospheric ventilation as a constraint on hurricane development and maintenance. Preprints, *Tech. Conf. on Hurricanes*, Miami Beach, FL, Amer. Meteor. Soc., D4-1–D4-10.

Sprintall, J., and M. Tomczak, 1992: Evidence of the barrier layer in the surface layer of the tropics. *J. Geophys. Res.*, **97**, 7305–7316, https://doi.org/10.1029/92JC00407.

Sun, J., G. Vecchi, and B. Soden, 2021: Sea surface salinity response to tropical cyclones based on satellite observations. *Remote Sens.*, **13**, 420, https://doi.org/10.3390/rs13030420.

Vincent, E. M., K. A. Emanuel, M. Lengaigne, J. Vialard, and G. Madec, 2014: Influence of upper ocean stratification interannual variability on tropical cyclones. *J. Adv. Model. Earth Syst.*, **6**, 680–699, https://doi.org/10.1002/2014MS000327.

Walker, N. D., W. J. Wiseman Jr., L. J. Rouse Jr., and A. Babin, 2005: Effects of river discharge, wind stress, and slope eddies on circulation and the satellite-observed structure of the Mississippi River plume. *J. Coastal Res.*, **216**, 1228–1244, https://doi.org/10.2112/04-0347.1.

Zedler, S. E., T. D. Dickey, S. C. Doney, J. F. Price, X. Yu, and G. Mellor, 2002: Analyses and simulations of the upper ocean's response to Hurricane Felix at the Bermuda testbed mooring site: 13–23 August 1995. *J. Geophys. Res.*, **107**, 3232, https://doi.org/10.1029/2001JC000969.

Zhang, X., R. D. Hetland, M. Marta-Almeida, and S. F. DiMarco, 2012: A numerical investigation of the Mississippi and Atchafalaya freshwater transport, filling and flushing times on the Texas-Louisiana shelf. *J. Geophys. Res.*, **117**, C11009, https://doi.org/10.1029/2012JC008108.

Zhang, Z., R. Hetland, and X. Zhang, 2014: Wind-modulated buoyancy circulation over the Texas-Louisiana shelf. *J. Geophys. Res. Oceans*, **119**, 5705–5723, https://doi.org/10.1002/2013JC009763.